Viscous Unsteady Flow around a Helicopter Rotor Blade in Forward Flight

Sharnappa, Vimala Dutta and P. K. Dutta
Computational and Theoretical Fluid Dynamics Division
National Aerospace Laboratories
Bangalore 560 017, INDIA
e-mail: pkd@ctfd.cmmacs.ernet.in, vimala@ctfd.cmmacs.ernet.in

Abstract

The unsteady three dimensional Reynolds averaged Navier-Stokes equations are solved for the moving domain in an inertial frame of reference to obtain time-accurate solution for the flow past a helicopter rotor blade in forward flight. The method uses an implicit dual time stepping procedure, a finite volume nodal point spatial discretisation and Baldwin-Lomax turbulence model. Results are presented for nonlifting and lifting cases. For the first case, the surface pressure distributions are found to be in good agreement with the experimental results at 89% of the rotor radius, except near the shock which is predicted to lie closer to the leading edge. In the lifting case, the surface pressure distributions compare well with the inviscid solution, both methods predicting the presence of a shock in the outboard region at the azimuth angle of 90°. However, the effect of viscosity here turns out to be to weaken the shock as well as to shift the shock position upstream.

Keywords: Unsteady flows, RANS solvers, Implicit schemes, Dual time stepping, Helicopter rotors

1 Introduction

The flow field around a helicopter rotor in forward flight is characterised by highly nonlinear three-dimensional unsteady viscous flow phenomena like transonic flow, shock-induced separation, vortex wake, dynamic stall and blade-vortex interaction. Some of these complexities persist even for an isolated rotor blade. Since the advancing and retreating blades operate under very different conditions, compressibility effects can be dominant on the advancing blade while separated flow may be present on the retreating blade. Consequently, the advancing blade is often characterised by shock formation on the suction (upper) surface and subsequent flow separation due to shock boundary layer interaction. In a loose sense, the flow field on the advancing blade can be modelled by using the two-dimensional blade element theory. The retreating blade, on the other hand, exhibits a chaotic flow field, particularly near the root since the trailing edge here faces the free stream. This often leads to flow separation on a massive scale and eventual dynamic stall. The strong tip vortex and the wake shed by a blade also affects the following blades thus leading to blade-vortex interaction. There is, however, one simplicity in the forward flight case, namely, reduced influence of the vortex wake on the flow field near the rotor since the free stream sweeps away the wake in the downstream direction. This is unlike a hovering rotor where the vortical wake remains close to the rotor and has considerable effect on the flow field near the rotor. The numerical simulation of such a complex flow situation calls for a high-resolution computation requiring the capability to compute transonic flows on the advancing blade and dynamic stall on the retreating blade.

In order to gain insight into the various fluid dynamical phenomena occurring over a helicopter rotor in forward flight, several time-accurate solutions of both Euler equations and Reynolds averaged Navier Stokes equations have been obtained in recent years [1-8]. Since computer run-times required for rotary-wing problems are much more than for a fixed-wing case, dual time method is often employed in the flow solvers. In this paper, an implicit finite volume nodal point scheme [9] with dual time stepping approach [10-14] has been used to simulate the flow over a helicopter rotor blade in forward flight. The numerical scheme is based on Euler's time differencing formula and a finite volume nodal point spatial discretisation wherein each control volume is obtained by joining the centroids of neighbouring cells surrounding the nodal point. The dual time stepping consists of an implicit discretisation in real time and the marching

of solution in a pseudo time to steady state at each physical time step. At each real time step of this dual time stepping procedure, an equivalent pseudo steady state problem is solved using local time stepping, which allows one to choose a very large physical time step based on accuracy requirements alone.

2 Computational Method

The Reynolds-averaged Navier-Stokes equations for three-dimensional unsteady compressible flow in a moving domain in nondimensional conservative form are given by

$$\frac{\partial \overline{U}}{\partial t} + \frac{\partial E}{\partial x} + \frac{\partial F}{\partial y} + \frac{\partial G}{\partial z} = 0. \tag{1}$$

Here, $\overline{U}$ is the vector of conserved variables, E, F and G are flux vectors, (x, y, z) is the Cartesian coordinate system and t is the time variable.

The governing equations (1) are solved by employing a dual time method with an implicit finite volume nodal point spatial discretisation [9,13,14]. Application of an implicit second order accurate backward difference formula for discretisation in real time and Euler's implicit time differencing formula for pseudo time leads to the following basic equation (2) of the implicit dual time stepping technique:

$$\left[I + \frac{3\Delta t^*}{2\Delta t} I + \Delta t^* \left(\frac{\partial R}{\partial U} \right)^m \right] \Delta U^m = -\Delta t^* \left[R(U^m) + \frac{3U^m}{2\Delta t} - \frac{2\overline{U}^n}{\Delta t} + \frac{\overline{U}^{n-1}}{2\Delta t} \right]. \tag{2}$$

Here $U^m = U(t^*) = U(m\Delta t^*)$ is the solution vector at pseudo time level m and $\Delta U^m = U^{m+1} - U^m$ is the change in U^m over the time step Δt^*, Δt denotes the real or physical time step that is required to resolve the physical unsteadiness of the flow. The barred quantities denote the solution vectors at the previous real time levels n and $n-1$ whereas R represents the spatial operators which give rise to the flux residual after a discretisation in space.

To facilitate the finite volume formulation, equations (2) are written in integral form and the surface integrals are evaluated by summing up the contributions due to the flux terms over the six faces of the computational cell. Applying integral conservative equations to each control volume, linearizing the changes in flux vectors using Taylor's series expansions in time, assuming locally constant transport properties, and dropping the superscript m we obtain

$$\left(I + \frac{3\Delta t^*}{2\Delta t} I \right) \Delta U_{ijk} + \frac{\Delta t^*}{\Omega_{ijk}} \sum_{m=1}^{6} \left\{ \left[\left(A - \frac{\partial E_R}{\partial x} \right) \Delta U \right]_m S_{mx} \right.$$

$$+ \left[\left(B - \frac{\partial F_S}{\partial y} \right) \Delta U \right]_m S_{my} + \left[\left(C - \frac{\partial G_T}{\partial z} \right) \Delta U \right]_m S_{mz} \right\}$$

$$= -\frac{\Delta t^*}{\Omega_{ijk}} \left\{ \sum_{m=1}^{6} \left[(E_I - E_V)_m S_{mx} + (F_I - F_V)_m S_{my} + (G_I - G_V)_m S_{mz} \right] \right\}$$

$$-\Delta t^* \left(\frac{3U_{ijk}}{2\Delta t} - \frac{2\overline{U}^n_{ijk}}{\Delta t} + \frac{\overline{U}^{n-1}_{ijk}}{2\Delta t} \right), \tag{3}$$

Here Ω_{ijk} is the control volume surrounding the nodal point (i, j, k) of the curvilinear grid; $A = \partial E_I / \partial U$, $B = \partial F_I / \partial U$, $C = \partial G_I / \partial U$, $E_R = \partial E_{V_1} / \partial U_x$, $F_S = \partial F_{V_2} / \partial U_y$ and $G_T = \partial G_{V_3} / \partial U_z$ are the Jacobian matrices; E_I, F_I and G_I are the inviscid flux vectors and E_V, F_V and G_V are the viscous flux vectors; S_{mx}, S_{my} and S_{mz} are the x, y and z components of the surface vector corresponding to the m-th surface of the control volume.

The terms containing inviscid flux vectors can be calculated by using the flow variables at the six neighbouring points and Taylor's series expansions can be utilised to discretise the derivatives in the

2

viscous flux terms directly in the physical plane. The resulting block tridiagonal system of equations are solved by using a suitable block tridiagonal solution algorithm and proper initial and boundary conditions. A blend of second and fourth order artificial dissipation terms [15] is added explicitly to ensure convergence and to suppress oscillations near shock waves. Implicit second order dissipation terms are also added to improve the practical stability bound of the implicit scheme. Turbulence closure is achieved through the algebraic eddy viscosity model of Baldwin and Lomax [16]. For a moving body, the equations are solved in the inertial frame of reference by employing a grid which remains fixed to the body and moves along with it. At each real time step $t + \Delta t$, starting from the solution at the previous time step t, the solution is marched in pseudo time t^* using local time stepping. Since the choice of physical time step Δt is no longer limited by stability considerations, a much larger time step, with a fixed but small number of inner iterations in pseudo time, can be used to reduce the undesirably large computational time for unsteady flow calculations. Based on this dual time stepping method an implicit Reynolds averaged Navier-Stokes solver IMPRANS has been developed at NAL for computing a wide range of three-dimensional unsteady viscous compressible flows. This RANS solver has been used to compute the unsteady flow over a rectangular helicopter rotor blade in forward flight under nonlifting and lifting conditions.

3 Results and Discussion

The schematic diagram of a helicopter rotor blade of radius R (a) in the plane of rotation zx or $z'x'$ and (b) in the sectional plane $x'y'$ is shown in Fig. 1(i). Here, the coordinate systems in the inertial and rotating frames of reference are denoted by (x, y, z) and (x', y', z') respectively and the rotation angles of the blade about the x', y' and z' axes are taken to be α, β and γ. These coordinate systems are chosen such that the axes x', y' and z' lie in chordwise, axial and spanwise directions with the origin of the system lying at the centre of rotation $c(x_c, y_c, z_c)$. The blade has a rectangular planform with uniform chord c and rotates about the y or y' axis with an angular velocity Ω in the presence of a free stream of velocity W_0 in the negative z direction. This is equivalent to a rotating blade moving with a forward velocity W_0 in the z direction. It may be noted that the blade pitch here is defined by the angle $-\gamma$ and, for a helicopter rotor blade in hover, $W_0 = 0$ since there is no forward velocity.

Results are presented for the unsteady flow over a blade of aspect ratio $R/c = 6$ with NACA 0012 aerofoil section. Here, the blade extends from $r/c = 1$ to 6 or $r/R = 1/6$ to 1 where r is directed along the blade span away from the centre of rotation, and the quarter-chord line of the blade is attached to the hub. This also implies that the root of the blade lies unit chord away from the axis of rotation. A physical time step $\Delta t = 0.010472$ (corresponding to about $0.1°$ rotation of the blade per time step) and a dual time stepping with 10 pseudo time steps are used. Computations are continued till the blade azimuth angle reaches $540°$ (or one and a half cycle) when the flow becomes almost periodic. A C-H grid of size $231 \times 65 \times 45$ is used for both the nonlifting and lifting cases presented here. Typical sectional grids at $r/R = 1.1$ and 0.5 generated by using the commercial software Gridgen are shown in Fig. 1(ii) to illustrate the typical grid structure at sections beyond the tip and on the blade. It may be noted that experimental investigation of a two-bladed model rotor, with each blade having the above configuration, was conducted by Caradonna and Tung [17] for hover condition and by Caradonna et al [18] for forward flight conditions. However, only the Euler calculation [4] is available for the lifting case.

Fig. 2 shows the time accurate solutions for the nonlifting case (pitch angle $-\gamma = 0$) with advance ratio $-W_0/\Omega R = 0.2$, tip Mach number $M_{\text{tip}} = 0.8$ and tip Reynolds number $Re_{\text{tip}} = 3.55 \times 10^6$. The temporal variations of the force coefficients $C_{x'}$, $C_{y'}$ and $C_{z'}$ along the x', y' and z' axes respectively and moment coefficients $C_{Mx'}$, $C_{My'}$ and $C_{Mz'}$ about the x', y' and z' axes respectively are shown in Fig. 2(i), where the region $\psi < 180°$ is taken from the region $360° < \psi < 540°$. The rapid fluctuations in $C_{y'}$ and $C_{Mx'}$ during the retreating stage are mainly the result of chaotic flow developed due to the free stream hitting the trailing edge. However, for this nonlifting case, all the coefficients are found to be very small. Fig. 2(ii) shows the surface pressure distributions at $r/R = 0.89$ for different azimuth angles. It is found that, for the advancing blade ($\psi < 180°$), the pressure distribution compares very well with the experimental pressure distribution [18], except near the shock. The shock here is predicted to

3

lie slightly upstream of the experimentally observed position. The Mach contours in the rotating frame of reference at the same radial station $r/R = 0.89$ are shown in Fig. 2(iii), illustrating the presence of a shock at about 60% of the chord. In conjuction with Fig. 2(ii), the shock is found to exist from $\psi = 60°$ to about $\psi = 150°$ at $r/R = 0.89$. The extent of the shock is illustrated more clearly in Fig. 2(iv) where the pressure contours are plotted on the blade surface. The figure shows that the shock begins to form at about $\psi = 45°$ and persists during most of the advancing stage till about $\psi = 180°$. The pressure contours in Fig. 2(iii) suggest that the blade sections behave like 2-D aerofoils during the advancing stage where the 2-D analysis of blade sections can possibily be used for design and analysis of helicopter rotor blades by using blade element theory.

Computed results for the lifting case with pitch angle $-\gamma = 8°$, advance ratio $-W_0/\Omega R = 0.3$, tip Mach number $M_{\text{tip}} = 0.628$ and tip Reynolds number $Re_{\text{tip}} = 3.55 \times 10^6$ are shown in Figs. 3 and 4. In the absence of any free-wake analysis, no correction was applied to the prescribed pitch angle. The force and moment coefficients, shown in Fig. 3(i), illustrate the fact that most of the forces and moments are generated by the advancing blade. The pressure distributions on the blade, at different radial stations r/R and three azimuth angles $\psi = 0°$, $90°$ and $270°$ are shown in Fig. 3(ii) to 3(iv). For $\psi = 90°$ and $270°$, these are compared with the Euler computation results [4] at $r/R = 0.8$, 0.89 and 0.96. It is found that the weak shocks, present in the outboard region ($r/R > 0.6$) at $\psi = 90°$, shift upstream due to viscous effect. There is, however, very little viscous effect on the retreating blade as may be inferred from Fig. 3(iv) for $\psi = 270°$. Fig 4 shows the Mach contours at different radial stations for $\psi = 90°$ and $270°$ and pressure contours on the blade surface at different azimuth angles ψ. As seen in Fig. 4(i), at $\psi = 90°$, the shock extends from $r/R = 0.6$ to the tip; this is further confirmed by Fig.4(iii). The shock forms close to the leading edge in the inboard region and gradually moves away towards the outboard region. Close to the tip, the shock again tends to move towards the leading edge.

4 Concluding Remarks

The complex unsteady flow over a helicopter rotor blade in forward flight is simulated through time-accurate computations using IMPRANS, a Reynolds averaged Navier-Stokes code. The implicit RANS solver is based on an indigenously derived implicit finite volume nodal point scheme and it incorporates dual time stepping to enhance its capability to handle problems requiring large CPU time. There is reasonably good agreement between the computed and measured data in the nonlifting case while the results for the lifting case compare well with the Euler computations except near the shock. Currently, the solver IMPRANS is being applied in the CFD analysis of the wind turbine blades.

References

1. Boniface, J. C. and Sides J. "Numerical Simulation of Steady and Unsteady Euler Flows Around Multibladed Helicopter Rotors", Proc. 19th European Rotorcraft Forum, Assocazione Italiana di Aeronautica e Astronautica, Rome,Vol.1, Sept.1993, pp C10-1 - C10-21.
2. Webster, R. S., Chen, J. P., Whitefield, D. L., "Numerical Simulation of a Helicopter Rotor in Hover and Forward Flight", AIAA Paper No. 95-0193, 1995.
3. Boniface J. C. and Pahlke K., "Calculations of Multibladed Rotors in Forward Flight Using 3-D Euler Methods of DLR and ONERA", Proc. 22nd European Rotorcraft Forum, Brighton, UK, Paper No. 58, Sept. 17-19, 1996.
4. Sheffer, S. G., Alonso, J. J., Martinelli, L. and Jameson, A., "Time Accurate Simulation of Helicopter Rotor Flows Including Aeroelastic Effects", AIAA Paper No. 97-0399, 1997.
5. Pahlke K. and Chelli E., "Calculations of Multibladed Rotors in Forward Flight Using a 3D Navier-Stokes Method", Proc. 29th European Rotorcraft Forum, The Hague, Netherlands, Paper No. 48, 2000.
6. Pomin, H. and Wagner, S., "Navier-Stokes Analysis of Helicopter Rotor Aerodynamics in Hover and Forward Flight", J. Aircraft, 39, 5, 2002, pp. 813-821.
7. Quiao, Z.D., Yang, A. M., Zhu, B., "Numerical Simlation of Navier-Stokes Equations for Helicopter Rotor in Forward Flight Using Moving Chimera Grids", ICAS 2002 Congress, 2002.

8. Allen, C. B., "An Unsteady Multiblock Multigrid Scheme for Lifting Forward Flight Rotor Simulation", Int. J. Numer. Meth. Fluids, 45:973-984, 2004.

9. Vimala Dutta, Dutta, P. K. and Sharanappa, "An Implicit RANS Solver for Unsteady Compressible Flow Computations", Proc. Seminar on State of the Art and Future Trends of CFD at NAL, NAL SP 0301, NAL, Bangalore, 2003.

10. Jameson, A., "Time Dependent Calculation Using Multigrid with Applications to Unsteady Flows past Airfoils and Wings", AIAA Paper 91-1596, 1991.

11. Heinrich, R., Pahlke, K. and Bleecke, H., "A Three Dimensional Dual-Time Stepping Method for the Solution of the Unsteady Navier-Stokes Equations", Proc. Unsteady Aerodynamics Conference, London, 1996, pp. 5.1-5.12.

12. Dubuc, L., Badcock, K. J., Richards, B. E. and Woodgate, M., "Implicit Navier-Stokes Simulations of Unsteady Flows", Proc. Unsteady Aerodynamics Conference, London, 1996, pp. 11.1-11.9.

13. Dutta P. K., Vimala Dutta, and Sharanappa, "Unsteady RANS Simulations Using Implicit Dual Time Stepping", Proc. Sixth Annual CFD Symposium, CFD Division of Aeronautical Society of India, Bangalore, August 11-13, 2003.

14. Vimala Dutta, Sharanappa, and Dutta P. K., "Navier-Stokes Computations for a Helicopter Rotor Blade in Hover.", Proc. Eighth Annual CFD Symposium, CFD Division of Aeronautical Society of India, Bangalore, August 11-13, 2005, CP 18.

15. Pulliam, T. H., "Implicit Solution Methods in Computational Fluid Dynamics", App. Num. Math., (Trans. IMACS), 2, 6, 1986, pp. 441-474.

16. Baldwin, B. S. and Lomax, H., "Thin Layer Approximation and Algebraic Model for Separated Turbulent Flows", AIAA Paper No. 78-257, 1978.

17. Caradonna, F. X. and Tung, C., "Experimental and Analytical Studies of A Model Helicopter Rotor in Hover,", NASA TM-81232, 1981.

18. Caradonna, F. X., Laub, G.H. and Tung, C., "An Experimental Investigation of the Parallel Blade-Vortex Interaction", NASA TM-86005, 1984.

(i) Schematic diagram
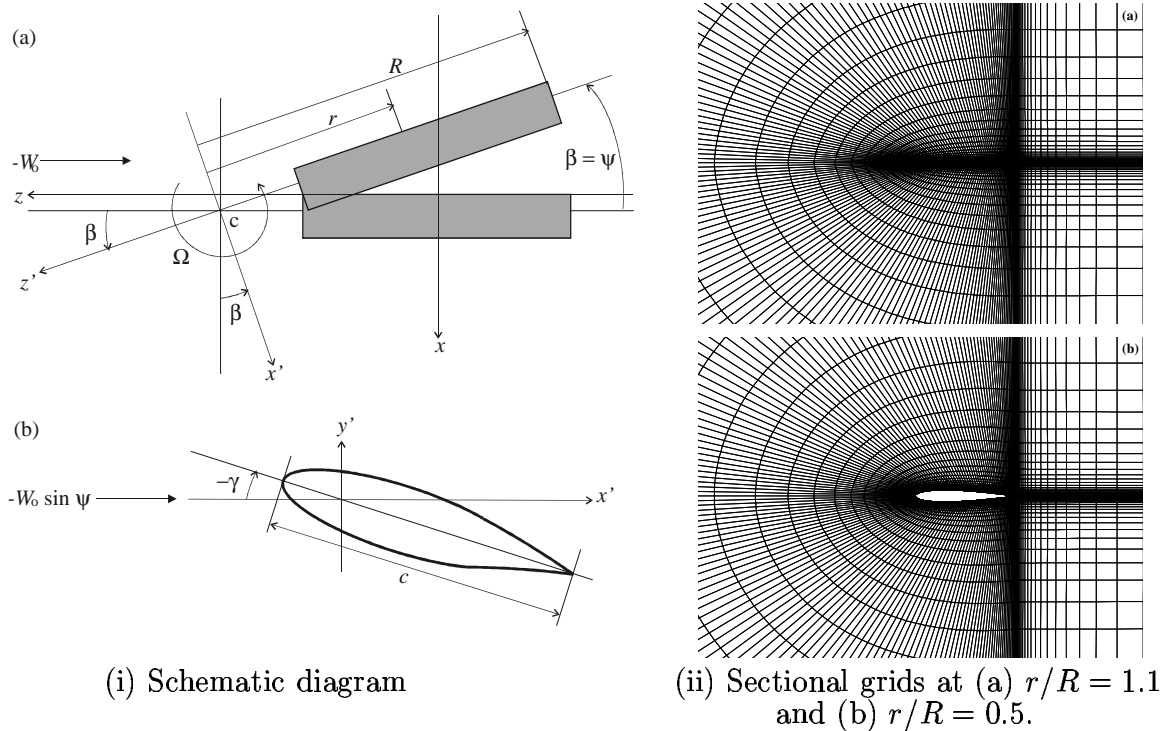
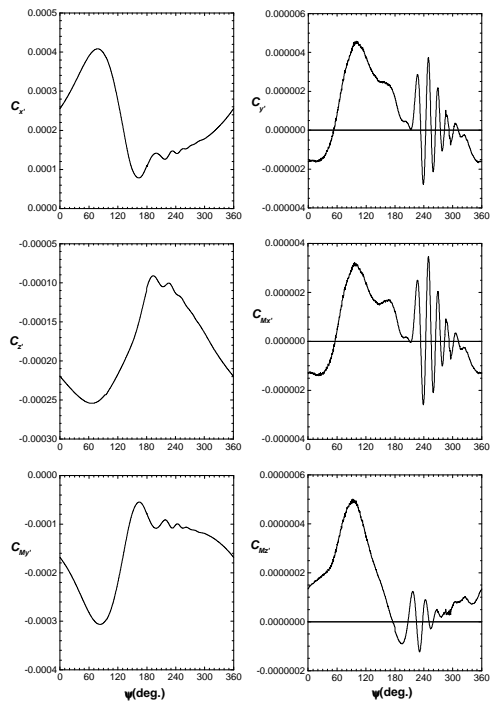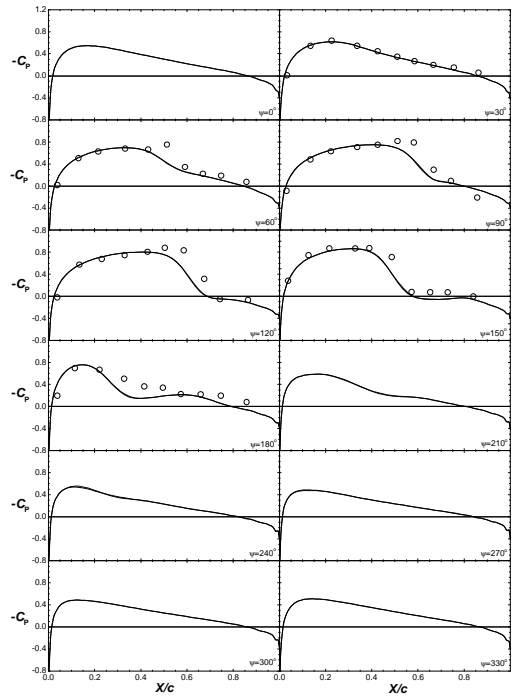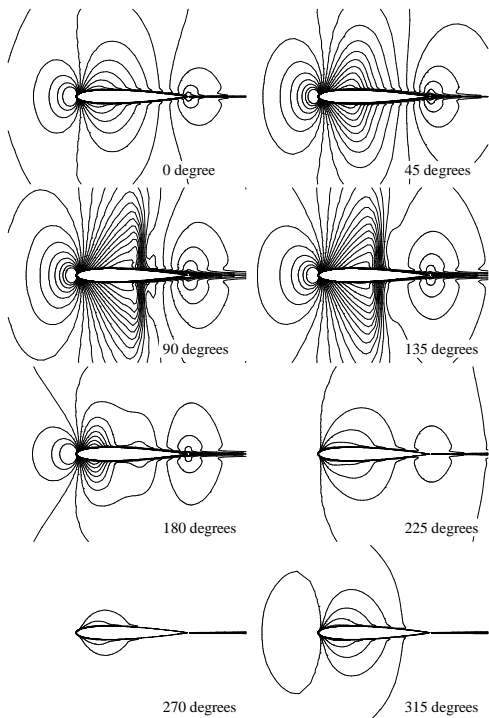(ii) Sectional grids at (a) $r/R = 1.1$ and (b) $r/R = 0.5$.

Fig. 1 Schematic diagram and grid for a rectangular rotor blade in forward flight. Aspect ratio $R/c = 6$; Section: NACA 0012 aerofoil.
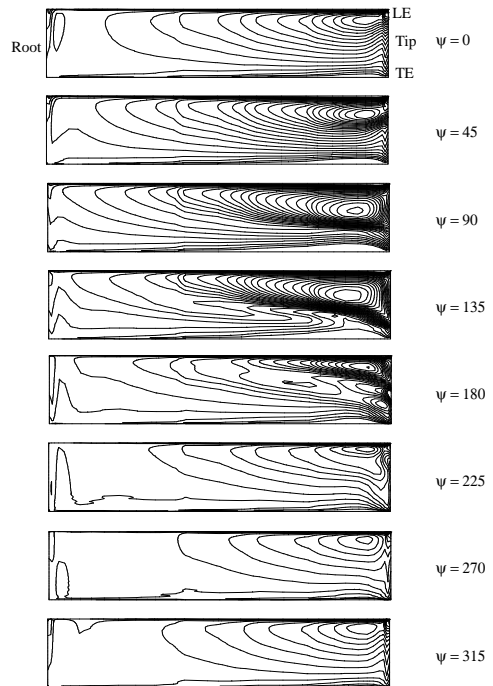
(i) Forces and moments

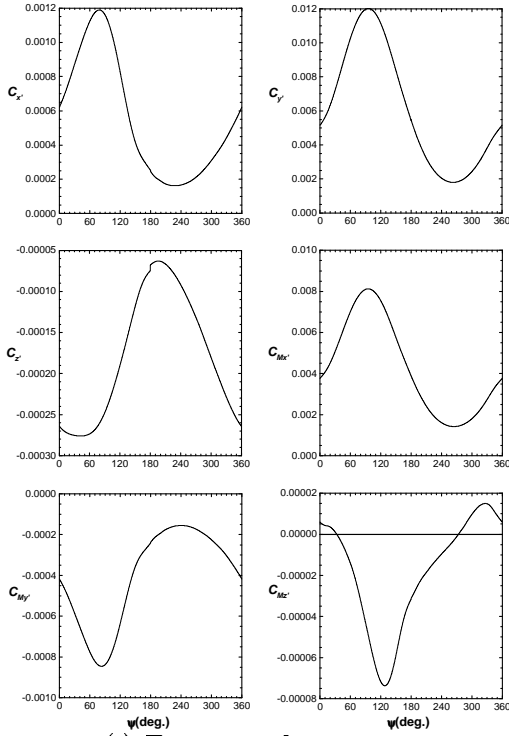(ii) Pressure distributions at $r/R = 0.89$
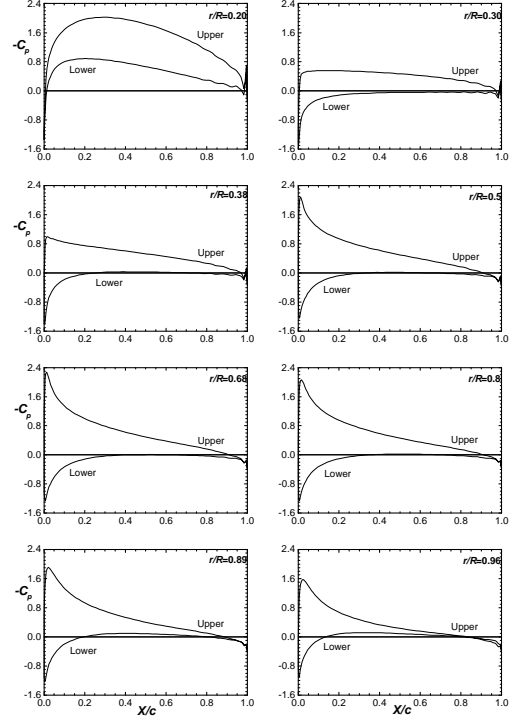
(iii) Relative Mach contours at $r/R = 0.89$
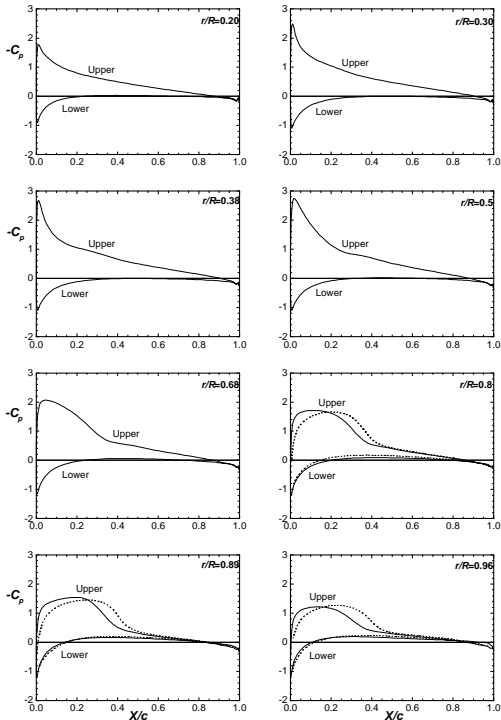
(iv) Pressure contours on blade surface

Fig. 2 Characteristics of a rectangular nonlifting rotor blade in forward flight. Aspect ratio $R/c = 6$;
Section: NACA 0012 aerofoil; $-W_0/\Omega R = 0.2$; $M_{tip} = 0.8$; $Re_{tip} = 3.55$ million.
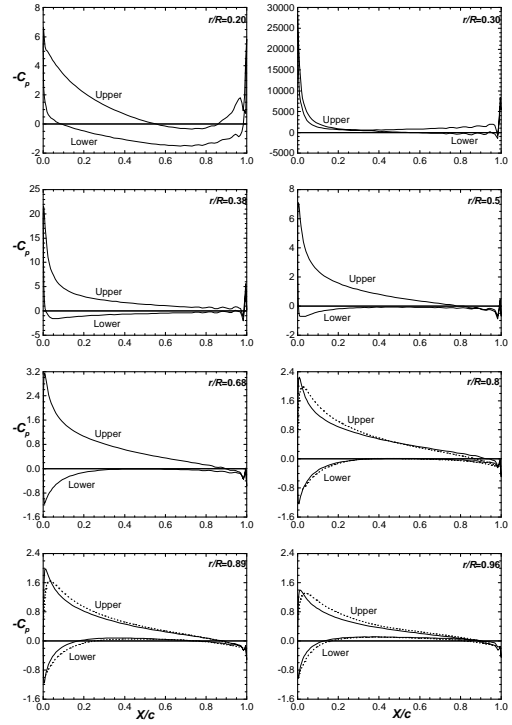o: Experimental pressure [18].

6

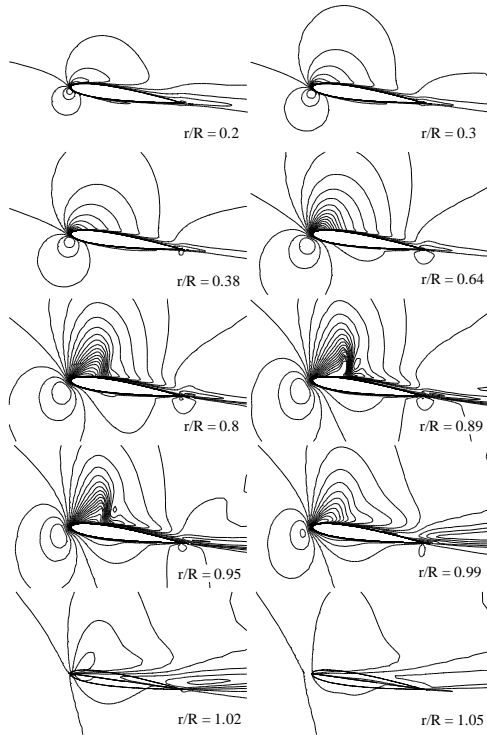(i) Forces and moments

(ii) Pressure distributions at $\psi = 0°$
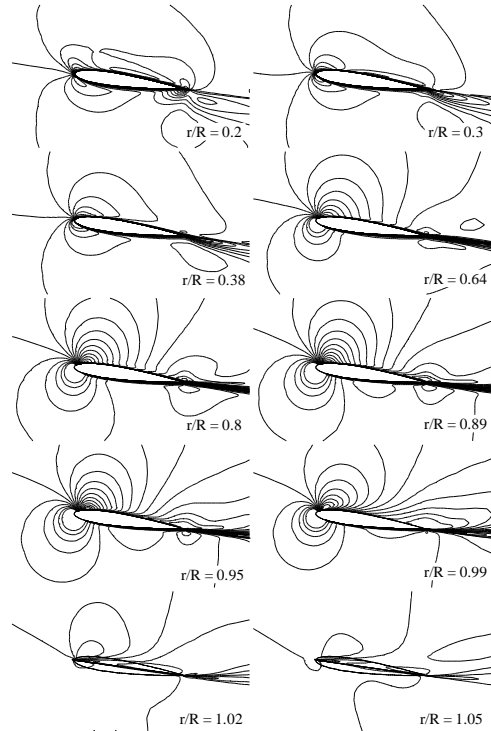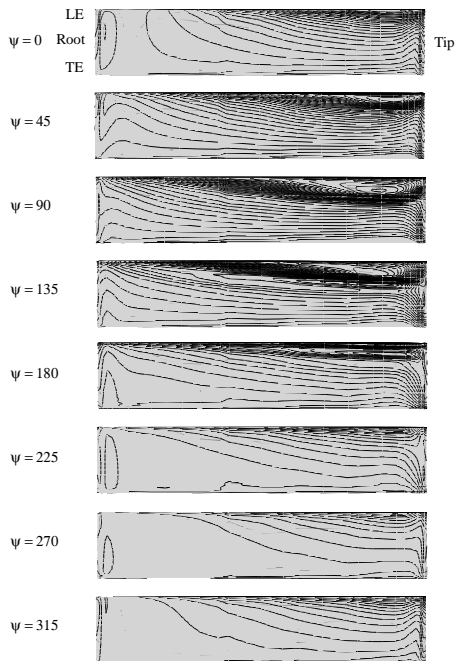
(iii) Pressure distributions at $\psi = 90°$

(iv) Pressure distributions at $\psi = 270°$

Fig. 3 Characteristics of a rectangular lifting rotor blade in forward flight. Aspect ratio $R/c = 6$; Section: NACA 0012 aerofoil; $-W_0/\Omega R = 0.3$; $M_{\text{tip}} = 0.628$; $Re_{\text{tip}} = 3.55$ million; $\gamma = -8°$. Dashed line: C_p distribution by Euler computation [4].
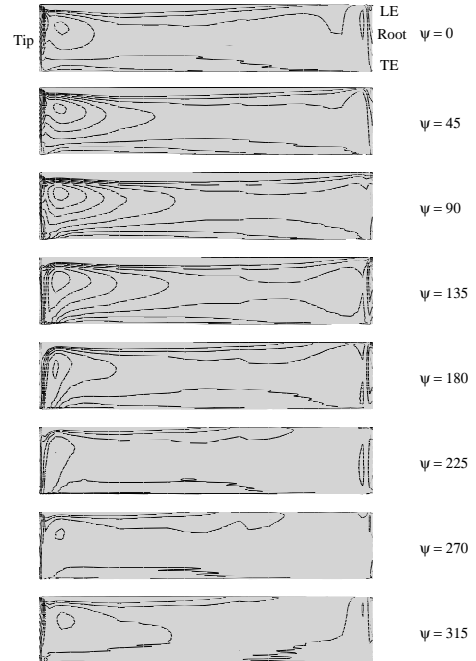
7

(i) Mach contours at $\psi = 90°$

(ii) Mach contours at $\psi = 270°$

(iii) Upper surface pressure contours

(iv) Lower surface pressure contours

Fig. 4 Mach and pressure contours on a rectangular lifting rotor blade in forward flight. Aspect ratio $R/c = 6$; Section: NACA 0012 aerofoil; $-W_0/\Omega R = 0.3$; $M_{tip} = 0.628$; $Re_{tip} = 3.55$ million; $\gamma = -8°$.